Thalamic transcranial electrical stimulation with temporal interference enhances sleep spindle activity during a daytime nap

Simone Bruno[1*], Beril Mat[1*], Erin L. Schaeffer[1,2], Ido Haber[1,3], Zhiwei Fan[1,4], Sean P. Prahl[1], Mackenzie R. Wilcox[1], Madelynn D. Loring[1], Tariq Alauddin[1], Richard F. Smith[1], Peter Achermann[5,6], Stefan Beerli[6], Myles Capstick[6], Esra Neufeld[6], Niels Kuster[6,7], William Marshall[8], Larissa Albantakis[1,9], Stephanie G. Jones[1,9], Chiara Cirelli[1,9#], Melanie Boly[1,9,10#], Giulio Tononi[1,9#]

Affiliations

1. Department of Psychiatry, University of Wisconsin-Madison, Madison, Wisconsin
2. Medical Scientist Training Program, University of Wisconsin-Madison, Madison, Wisconsin
3. Department of Biomedical Engineering, University of Wisconsin-Madison, Madison, Wisconsin
4. International Institute for Integrative Sleep Medicine (WPI-IIIS), Tsukuba Institute for Advanced Research (TIAR), University of Tsukuba, Tsukuba, Japan
5. Institute of Pharmacology and Toxicology, University of Zurich, Zurich, Switzerland
6. Foundation for Research on Information Technologies in Society (IT'IS), Zurich, Switzerland
7. Department of Information Technology and Electrical Engineering, Swiss Federal Institute of Technology (ETH) Zurich, Zurich, Switzerland
8. Department of Mathematics and Statistics, Brock University, St. Catharines, Ontario, Canada
9. Wisconsin Institute for Sleep and Consciousness, University of Wisconsin-Madison, Madison, Wisconsin
10. Department of Neurology, University of Wisconsin-Madison, Madison, Wisconsin

* These authors equally contributed to this work
# These authors share last authorship

Corresponding author:

Giulio Tononi, Department of Psychiatry, University of Wisconsin-Madison, Madison, Wisconsin, gtononi@wisc.edu

Abstract

Introduction: Sleep spindles are electroencephalographic elements characteristic of non-rapid eye movement sleep generated by thalamo-cortical interactions. Spindles have been linked to some of the cognitive benefits afforded by sleep and high spindle activity is associated with increased arousal threshold (deeper sleep). Here, we demonstrate that targeting the thalamus with Transcranial Electrical Stimulation with Temporal Interference (TES-TI) can enhance spindle activity.

Methods: 24 participants (25.5 ± 9.5 years; 69.6% F) underwent thalamic TES-TI stimulation during daytime naps. Three stimulation protocols were tested during stage 2 of non-rapid eye movement sleep (N2): fixed difference frequency of 10 Hz (TES^{15kHz}-TI^{10Hz}), difference frequency matched to individual spindle peak (TES^{15kHz}-TI^{Peak}), and carrier frequency only (TES^{15kHz}). Spectral power in the spindle (sigma) band and integrated spindle activity (ISA) were compared before and during the stimulation, and across stimulation protocols.

Results: TES^{15kHz}-TI^{10Hz} stimulation was associated with a significant increase in sigma band power ($\Delta\tilde{x}_{STIM-PRE}$ = 0.49 $log_{10}\mu V^2$, p = 0.021) and ISA ($\Delta\tilde{x}_{STIM-PRE}$ = 7.48 μV/s, p = 0.042). Cluster-based analysis localized the increase in sigma power over the frontal and centro-parietal areas (p = 0.022). Linear mixed effects models showed that both sigma band power and ISA during stimulation increased significantly in TES^{15kHz}-TI^{10Hz} compared to the TES^{15kHz} protocol (β = 0.67 $log_{10}\mu V^2$, p = 0.018; β = 14.70 μV/s, p = 0.0077), while the TES^{15kHz}-TI^{Peak} did not show the same effect.

Conclusions: This study provides evidence supporting the successful use of TES-TI targeting the thalamus to enhance sleep spindle activity. Stimulation at a fixed difference frequency of 10 Hz increased sigma band power and ISA, whereas neither stimulation matched to individual sigma band peak nor TES alone

produced comparable effects. These promising results warrant further investigations into the cognitive and clinical impact of TES-TI, a non-invasive neuromodulation tool that can reach deep brain regions.

Keywords: Sleep spindles; Sleep; Non-REM; Thalamus; Thalamo-cortical network; Temporal interference stimulation; Transcranial electrical stimulation; Non-invasive brain stimulation; High-density electroencephalography

Statement of significance

This study provides evidence that thalamo-cortical networks, which are central to many physiological and pathological brain activities, can be modulated non-invasively in humans. More specifically, the findings show that transcranial electrical stimulation with temporal interference targeting the thalamus can selectively enhance sleep spindle activity. This work introduces a new strategy for precisely targeting sleep-generating mechanisms regulated by deep brain circuits without surgery or medication. Key next steps include determining how this increase in spindle activity can positively impact cognition and assessing the translational potential of this approach for clinical populations.

Introduction

Sleep spindles are transient, burst-like electroencephalographic (EEG) features that serve as a defining characteristic of non-rapid eye movement (NREM) sleep in mammals. First identified by Loomis and colleagues[1], they were named for their distinctive waxing-and-waning morphology. In human adults, sleep spindles typically show oscillations within the 11–16 Hz frequency range, representing the most important contributor to the EEG sigma band power. Slow (<13 Hz) and fast (> 13 Hz) spindles are preferentially found in the frontal and centro-parietal neocortex, respectively[2,3]. Sleep spindles first emerge at the onset of stage N2 sleep and continue to occur into stage N3, where their density and detectability decline[4]. Evidence from animal model studies has also demonstrated a role for sleep spindles in guiding the transition from NREM to REM sleep via a transitional stage, the EEG power spectrum of which is characterized by increased sigma band power relative to both NREM and REM sleep[5,6]. At the cellular level, spindle activity originates in the thalamus. Specifically, the thalamic reticular nucleus represents the spindle pacemaker and its rhythmic interactions with the thalamocortical relay neurons constitute the core neurophysiological mechanism underlying spindle generation[2,7].

Growing evidence indicates that sleep spindles, alone or in coordination with other sleep-related oscillations[8], support sensory gating[2] and memory consolidation[9]. Sleep spindles deficits have been reported in patients affected by schizophrenia[10], Alzheimer disease[11], Parkinson disease[12] and epilepsy[13], in association with decreased cognitive abilities, thus representing a potential biomarker and treatment target[14].

Efforts to enhance sleep spindle activity have employed both pharmacological[15] and non-invasive brain stimulation approaches[16]. Among central nervous system-active compounds, benzodiazepines and Z-drugs have demonstrated the most robust effects in increasing spindle activity[15], with associated improvements in memory consolidation[17]. However, their clinical utility is limited by adverse effects, including dependence, cognitive impairment, and suppression of slow wave sleep[18]. Acoustic stimulation in the sigma

frequency range has also been explored, though results have been inconsistent[19,20]. Moreover, auditory stimulation presents practical challenges, as the thalamo-cortical system is highly sensitive to acoustic stimuli during sleep[21], which may elicit unintended awakenings. Transcranial Alternating Current Stimulation (tACS), when applied bifrontally at 12 Hz in phase with endogenous spindles, can enhance post-stimulation spindle activity[22]. Despite this, tACS is suboptimal for spindle modulation due to its limited ability to target deep brain structures such as the thalamus without causing significant discomfort to the participant. Additionally, the artifact introduced by conventional TES precludes the acquisition of EEG data temporally synchronized with the stimulation.

Transcranial Electrical Stimulation with Temporal Interference (TES-TI) can address the limitations inherent in conventional non-invasive brain stimulation techniques. This approach employs the superposition of two high-frequency signals, in the range of kHz, with slightly different frequencies (carriers). Their interaction produces an interference pattern characterized by amplitude modulation of the electric field at the difference frequency[23]. The difference frequency can target neural tissue within a region of interest (ROI) throughout the depth of the brain with higher focality compared to standard TES[24]. Moreover, the use of kHz carriers can virtually eliminate local sensation and discomfort[25,26], and therefore the risk of awakening subjects during sleep.

In this study, we show how TES-TI can be effectively applied to target the thalamus without disrupting sleep. Through concurrent high-density EEG (hd-EEG) recordings enabled by custom hardware, we show that TES-TI produces a significant enhancement of sleep spindle activity.

Materials and Methods

Experimental design

Data for this study were collected during Phase I of the REM REST clinical trial (NCT06547086), a single-blind longitudinal study aimed at identifying the most effective TES-TI stimulation parameters for eliciting sleep spindles and sawtooth waves during daytime sleep episodes, with the ultimate goal of enhancing emotional well-being and stress resilience.

During the initial (baseline) visit to the Wisconsin Sleep Center, participants were fitted with an hd-EEG net and given the opportunity to take a 90-minute nap. EEG data from the baseline session were used to determine each participant's individual sigma peak frequency, defined as the 0.5 Hz frequency bin with the highest power within the 11–16 Hz range.

Participants who successfully slept during the baseline nap underwent an MRI session, during which T1- and T2-weighted structural images were acquired. These images were used to optimize electrode placement for TES-TI stimulation, maximizing both intensity and focality of thalamic targeting. Stimulating electrodes were embedded in the hd-EEG net replacing recording electrodes.

In two subsequent visits, participants received the following stimulation protocols during NREM sleep, presented in randomized order:

- TES-TI, with a 10 Hz difference frequency (TES^{15kHz}-TI^{10Hz})
- TES-TI, with a difference frequency matched to the individual sigma peak (TES^{15kHz}-TI^{Peak})
- TES, at carrier frequency (TES^{15kHz})

Only stimulation intervals entirely included in sleep stage N2, as identified during offline sleep staging, were included in the analysis. Intervals were required to be at least 90 seconds in duration after artifact removal and to be preceded by a minimum of 3 minutes of continuous N2 sleep. Post-stimulation intervals were not included in the present analysis. Indeed, for approximately 50% of the stimulation intervals

delivered during N2 sleep, the stimulation period was followed by a transition to a different sleep stage (mainly N3). The reduced number of stimulation intervals followed by the N2 sleep stage made it difficult to distinguish post-stimulation effects from changes attributable to the transition in sleep stage. Additional stimulations, whose results are not included in the present paper, were applied during REM sleep and wakefulness using different stimulation parameters and/or targets.

All participants provided written informed consent prior to participation. The study was conducted in accordance with the Helsinki Declaration and approved by the Institutional Review Board of the University of Wisconsin–Madison on 5/28/2024 (ID: 2024-0352).

Study participants

Eligible participants were English-speaking, medically healthy adults aged 18–50 years who reported habitually taking more than one nap per week and had no history of neurological or sleep disorders.

Exclusion criteria were as follows:

- Any current or past history of neurological disorders or acquired neurological disease (e.g. stroke, traumatic brain injury), including intracranial lesions
- History or head trauma resulting in prolonged loss of consciousness
- History of more than 1 >3 grade head concussion
- Current history of poorly controlled headaches, including intractable or poorly controlled migraines
- Any systemic illness or unstable medical condition that may cause a medical emergency in case of a provoked seizure (cardiac malformation, cardiac dysrhythmia, asthma, etc)

- History of seizures, diagnosis of epilepsy, history of abnormal (epileptiform) EEG, or family history of treatment resistant epilepsy, with the exception of a single seizure of benign etiology (e.g., febrile seizures) in the judgment of a board-certified neurologist
- Possible pregnancy or plan to become pregnant in the next 6 months
- Any metal in the body
- Any medical devices or implants (i.e., cardiac pacemaker, medication infusion pump, cochlear implant, vagal nerve stimulator) unless otherwise approved by the responsible MD
- Dental implants containing metal
- Any medication that may alter seizure threshold: ADHD stimulants (Adderall, amphetamine); tricyclic/stypical antidepressants (amitriptyline, doxepine, imipramine, maprotiline, nortriptyline, buproprion); antipsychotics (chlorpromazine, clozapine); bronchodilators (theophylline, aminophylline); antibiotics (fluoroquinolones, imipenem, penicillin, cephalosporins, metronidazole, isoniazid); Antivirals (valacyclovir, ritonavir); OTC antihistamines (diphenhydramine, Benadryl)
- Claustrophobia
- Back problems that would prevent lying flat for up to two hours
- Regular night-shift work (second or third shift)

EEG data acquisition and preprocessing

EEG data were collected using the Magstim Electrical Geodesics Inc. (EGI) system equipped with 256 silver-silver chloride electrodes, referenced to Cz. Data acquisition and real-time monitoring were performed using EGI Net Station software, which enabled experimenters to visualize EEG activity and initiate stimulation based on sleep stage. For sleep staging purpose, the EEG montage included additional

electrodes for polysomnographic recordings: electrooculography, recorded using two electrodes placed adjacent to the outer canthi, each referenced to the contralateral mastoid; electromyography, recorded using a pair of electrodes positioned in the submental region; electrocardiography, recorded using two electrodes placed below the clavicle and on the contralateral side of the rib cage. An optical trigger box was connected to both the TES-TI stimulator and the EGI amplifier, marking the onset and offset of stimulation periods to enable precise offline identification of stimulation intervals. All signals were sampled at 500 Hz.

Sleep staging was performed by a registered sleep technician in accordance with the most recent guidelines of the American Academy of Sleep Medicine (AASM)[4], using the open-source MATLAB-based software CountingSheepPSG[27].

EEG data preprocessing was conducted using a custom MATLAB routine that incorporated functions from the EEGLAB toolbox[28]. EEG data were bandpass filtered between 0.5 and 40 Hz Hz applying a zero-phase, forward-and-reverse finite impulse response filter using the EEGLAB's *pop_eegfiltnew* function. Bad channels were identified through visual inspection of the EEG time series and additional topography-based procedures. Channels corresponding to electrodes that were replaced by stimulation electrodes were also excluded. Artifact-contaminated segments were manually identified and removed following visual inspection of the EEG signal. Analyses were restricted to the central 185 scalp EEG channels. Any channels within this subset that were previously removed were interpolated using spherical spline interpolation before average referencing.

Power spectral density was calculated with Welch's method using 6-second windows with 90% overlap. EEG power bands were defined as follows:

- Delta: 0.5-4 Hz
- Theta: 4-8 Hz
- Sigma: 11-16 Hz

- Beta: 16-25 Hz
- Gamma: 25-40 Hz

MRI data acquisition

A 3 Tesla MAGNUS (Microstructure Anatomy Gradient for Neuroimaging with Ultrafast Scanning, GE Healthcare) head-only scanner was used to acquire MRI data. T1- and T2-weighted sequences captured brain structural images with the following parameters:

- T1:
    - sequence = MP-RAGE (Magnetization-Prepared Rapid Gradient-Echo)
    - repetition time (TR) = 2000 ms
    - echo time (TE) = 3 ms
    - field of view (FOV) = 256 x 256 mm^2
    - inversion time (TI) = 1100 ms
    - flip angle = 8 degrees
    - number of slices = 240
    - resolution = 0.8 mm x 0.8 mm x 0.8 mm
    - matrix size = 320 x 320 pixels
    - acquisition time = 4 minutes.

- T2:
    - sequence = CUBE-T2
    - TR = 2500 ms
    - TE = 90 ms
    - FOV = 256 x 256 mm^2

- echo train length (ETL) = 120
- number of slices = 240
- resolution = 0.8 mm x 0.8 mm x 0.8 mm
- matrix size = 320 x 320 pixels
- acquisition time = 4 minutes.

TES-TI setup

Silver-silver chloride ceramic electrodes (outer diameter: 12.6 mm; inner diameter: 8.0 mm; width: 2.2 mm) were embedded into the hd-EEG net, replacing standard recording electrodes, and connected to the TI Brain Stimulator for Research (TIBS-R v3.0, TI Solutions AG, Switzerland) for stimulation delivery. Electrode-skin impedance of the stimulating electrodes was continuously monitored and maintained between 4 and 6 kΩ throughout the experiment.

TES-TI was administered using a carrier frequency of 15 kHz. When a multipolar montage was employed, a carrier frequency of 17 kHz was selected for the second pair of stimulation channels[29]. Three stimulation protocols were tested: (1) TES-TI with a 10 Hz difference frequency (TES^{15kHz}-TI^{10Hz}), (2) TES-TI with a difference frequency matched to the participant's individual sigma peak (TES^{15kHz}-TI^{Peak}), and (3) TES without a difference frequency, that is, only carrier frequency (TES^{15kHz}). As a further control condition for the deepening of sleep during the nap, two consecutive 3-minute intervals of N2 sleep were selected from the baseline nap and compared (No Stimulation condition). To make the no stimulation condition comparable to the stimulation protocols, N2 consecutive 3-minute intervals were randomly selected from different parts of the nap, choosing them at varying time distances from sleep onset. Their number approximately matched the number of stimulation intervals analyzed in the other stimulation protocols. All stimulation protocols employed sinusoidal waveforms and were delivered for 3 minutes with two 15-

second ramp-up and ramp-down periods. Stimulation intensity was set to the highest level that did not produce any scalp sensation, up to a maximum of 8 mA peak-to-peak.

Hardware filters placed between the stimulator output and the EEG amplifier eliminated electrical noise from the stimulator, ensuring artifact-free EEG recordings during stimulation. A full description of the setup can be found in Schaeffer et al., 2025[30].

Optimization of stimulating electrodes placement

Electrode placement was individualized for each participant using TI-Toolbox[31], an open-source platform for temporal interference research. The toolbox comprises four modules: preprocessing, optimization, simulation, and analysis.

1. Preprocessing: Individualized head models were generated from structural MRI data. DICOM images were first converted to NIfTI volumes and subsequently transformed into meshed volumes conductors using the *charm* function. Tissue-specific conductivity values were assigned to the different tissues, assuming isotropic conductivities throughout the head model. As part of the preprocessing pipeline, the GSN-HydroCel-256 net was automatically co-registered to each individual head model using a non-linear registration from MNI space.
2. Optimization: The optimal electrode montage for targeting both thalami was determined using genetic and/or local exhaustive search algorithms introduced by Haber and colleagues. Stimulation electrodes placement was optimized to maximize the temporal interference electric field at target and minimize it outside the ROI.
3. Simulation: Electric field distributions and TI patterns were computed for the montage(s) identified in Step 2. Electric field values within gray matter were extracted and visualized on both the participant's native T1-weighted MRI and the standardized MNI152 atlas.

4. Analysis: Intensity and focality metrics were calculated for the thalami. Intensity was defined as the mean TI electric field within the ROI, and focality as the ratio of the mean TI electric field in the ROI to that in the remaining gray matter. The montage providing the best trade-off between intensity and focality was selected for each participant.

Sleep spindle detection

Sleep spindles were detected using the open-source Python library YASA[32], which implements an algorithm inspired by the method originally described by Ferrarelli et al.[10] and Lacourse et al.[33]. EEG data were first bandpass-filtered within the spindle frequency range (Sigma band: 11–16 Hz). Spindle detection was then based on three complementary features:

- Root Mean Square (RMS): the RMS of the filtered signal was computed using a sliding window of 300 ms with a 100 ms step size;
- Band-Specific Correlation: a moving correlation was calculated between the broadband EEG signal and the spindle-band filtered signal, using the same windowing parameters;
- Relative Spectral Power: the proportion of power in the sigma band relative to the total power was estimated using Short-Time Fourier Transform with 2-second windows and 200 ms overlap.

A spindle was detected when the following criteria were simultaneously met:

- the RMS exceeded the mean RMS plus 1.5 times the RMS of successive differences;
- the moving correlation exceeded 0.65;
- the relative sigma power was greater than 0.2.

Events with durations shorter than 0.3 seconds or longer than 2.5 seconds were excluded, regardless of whether they met the detection criteria. Only spindles detected in at least 2 channels were included, while events occurring within 500 ms of each other were considered as the same event.

To comprehensively capture the full spectrum of spindle activity, spindle detection was separately performed across two frequency ranges: 11-13.5Hz and 13-16Hz. The resulting spindle events were subsequently merged, and in cases of overlap, only the longer spindle was retained. Integrated spindle activity (ISA) was selected as a primary outcome because it provides a unified measure of multiple spindle characteristics, i.e., amplitude, density, and duration, thereby offering a comprehensive representation of spindle activity within the interval of interest. ISA was computed for both the STIM and PRE intervals by integrating the absolute amplitude in the sigma band range of each detected spindle across all electrodes and normalizing the resulting value by the duration of the interval[10].

Statistical analysis

Quantitative variables were summarized using the median ($\tilde{x}$) and interquartile range, while categorical variables were described using frequencies and percentages. The Kruskal-Wallis test was performed to assess potential differences in age and sleep-related metrics across experimental conditions. Fisher's exact test was used to evaluate differences in gender, race, and ethnicity across stimulation protocols. The Wilcoxon signed-rank test was employed to compare: average band power and ISA during stimulation (STIM) and the preceding three-minute (PRE) (paired); and intensity and focality of the interference electric field in the thalami in TES^{15kHz}-TI^{Peak} and TES^{15kHz}-TI^{10Hz} protocols. For topographical comparisons, a cluster-based nonparametric statistical approach was used[34], based on the method described in Fattinger et al.[35]. Mixed-effects linear regression models were fitted to compare the increase (STIM-PRE) in sigma power and ISA in the TES^{15kHz}-TI^{10Hz} protocol compared to the active control TES^{15kHz}-TI^{Peak} and TES^{15kHz} protocols. Analyses were performed using R version 4.4.1, MATLAB 2024a, and Python 3.10.6. All statistical tests were two-sided, with a significance threshold set at $p < 0.05$.

Results

Descriptive statistics of the sample

A total of 24 participants were enrolled in the study. After the initial visit, during which hdEEG data were collected during a nap, participants returned for two additional sessions in which TES-TI targeting the thalamus bilaterally and TES protocols were delivered during N2 sleep in random order (Figure 1).

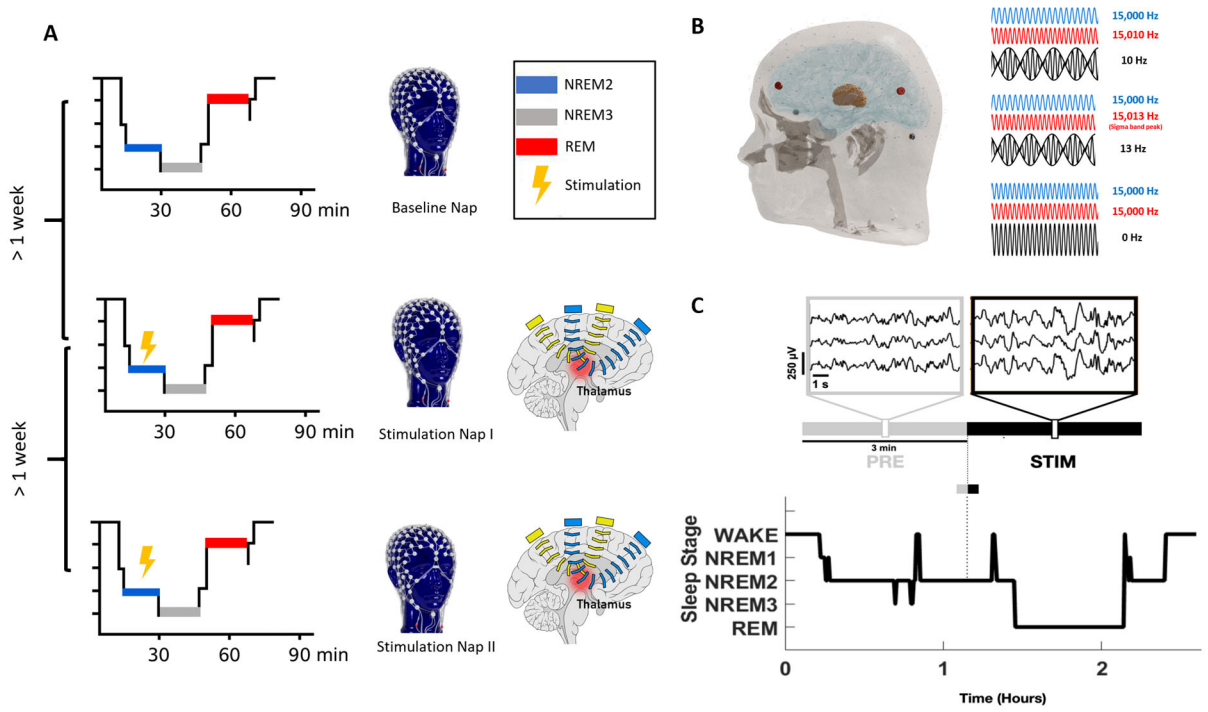

Figure1. Experiment design. A, During this first visit, high-density EEG was recorded without stimulation (Baseline Nap). Two additional visits, scheduled at least one week apart, followed the same procedure but included TES-TI bilaterally targeting the thalamus and TES stimulation protocols during N2 sleep (Stimulation Nap I and II). **B,** Representative stimulating electrodes' location for thalamic targeting and a schematic representation of the stimulation frequencies. **C,** Example of a stimulation protocol delivered during a Stimulation Nap. Only protocols where both STIM and PRE occurred entirely within N2 sleep were included in the analysis.

Stimulation electrode placement was optimized individually for each participant using head models derived from their T1 and T2-weighted MRI scans (Figure 2A).- and T2-weighted MRI scans

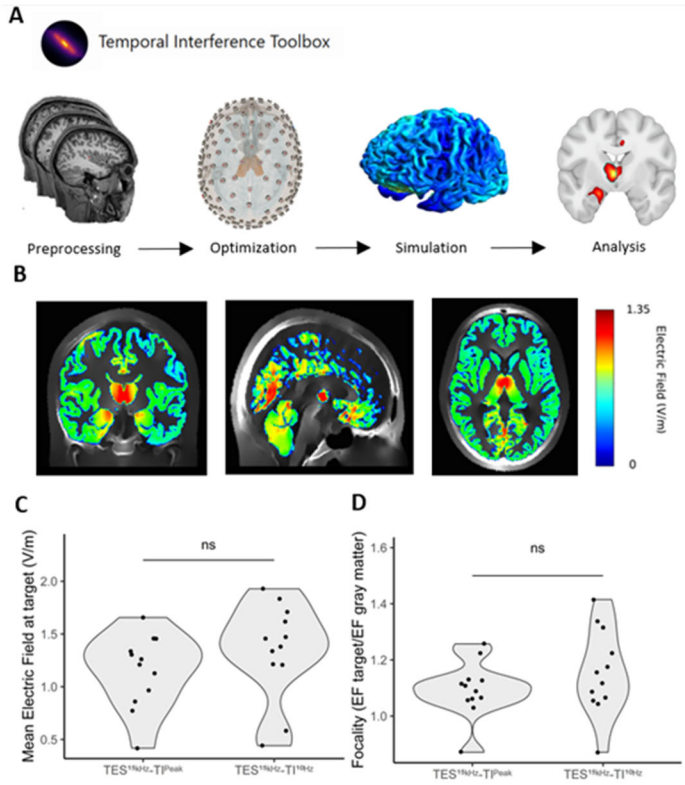

Figure 2. Individual optimization of stimulating electrode placement. A, individualized head models were generated from T1- and T2-weighted MRI scans (Preprocessing). Electrode placement was optimized to maximize the temporal interference electric field in the thalami and minimize it outside the region of interest (Optimization). Electric field distribution across gray matter was visualized to confirm adequate stimulation of the target (Simulation). Intensity and focality of electric field were quantified for each participant (Analysis). **B,** distribution of the simulated temporal interference electric field within the gray matter of a participant of the study, visualized in MNI space. Average temporal interference electric field in the thalami (**C**) and focality of the stimulation (**D**) under two conditions: TES^{15kHz}-TI^{10Hz} and TES^{15kHz}-TI^{Peak} frequency; No significant difference between the two stimulation protocols was found (Wilcoxon test, $p > 0.05$).

Only stimulation intervals that were entirely included within the N2 sleep stage and preceded by 3 minutes of N2 sleep were included in the final analysis. As a result, not all participants contributed data to every stimulation protocol. The final distribution was as follows: 12 participants for the TES^{15kHz}-TI^{10Hz} protocol, 12 for the TES^{15kHz}-TI^{Peak} protocol, and 10 for the TES^{15kHz} protocol. Similarly, 12 participants were included in the baseline condition.

Participants' median age was 24.0 years ± 9.5 ys, and 69.6% of participants were female. No significant differences were observed across experiment conditions in demographic variables, sleep duration, sleep quality, or sleep macroarchitecture. Results are fully displayed in Table 1.

Table 1. Descriptive statistics of the sample. No significant differences were found in demographic or sleep-related variables across the stimulation protocols groups.

		TES^{15kHz}-TI^{10Hz}	TES^{15kHz}-TI^{Peak}	TES^{15kHz}	No stimulation	P value
N		12	12	10	12	
Age (ys)		28.00 [23.50, 33.25]	23.50 [21.00, 25.50]	28.50 [24.75, 31.75]	23.50 [21.00, 29.25]	0.260
Gender						
	Female	8 (66.7%)	6 (50.0%)	8 (80.0%)	8 (66.7%)	0.588
	Male	4 (33.3%)	6 (50.0%)	2 (20.0%)	4 (33.3%)	
Ethnicity						
	Hispanic	0 (0%)	1 (8.3%)	1 (10%)	1 (8.3%)	0.886
	Non-Hispanic	12 (100.0%)	11 (91.7%)	9 (90%)	11 (91.7%)	
Race						
	Asian	3 (25.0%)	2 (16.7%)	1 (10.0%)	1 (8.3%)	0.814
	White or Caucasian	9 (75.0%)	10 (83.3%)	9 (90.0%)	11 (91.7%)	
Sleep Duration (min)		86.50 [70.00, 110.75]	92.00 [64.38, 100.69]	84.75 [68.38, 107.25]	91.75 [85.50, 100.38]	0.989
Sleep Efficiency (%)		74.92 [66.82, 89.87]	82.03 [63.30, 89.42]	83.49 [64.88, 87.29]	72.88 [61.43, 83.86]	0.815
Wake After Sleep Onset (min)		13.75 [5.90, 24,88]	19.50 [5.88, 44.16]	19.50 [9.96, 25.00]	28.00 [12.12, 53.00]	0.601
Number of Arousals		6.00 [4.00, 6.62]	7.25 [4.75, 11.00]	7.50 [5.00, 10.75]	10.50 [6.00, 13.25]	0.183
N1 (min)		8.50 [6.50, 9.38]	6.00 [4.00 8.50]	13.50 [8.25, 18.00]	9.00 [2.75, 11.25]	0.221
N1 (%)		9.96 [6.94, 13.94]	9.85 [4.50, 14.14]	14.59 [11.04, 21.31]	9.17 [2.49, 19.05]	0.472
N2 (min)		55.50 [42.75, 64.25]	44.50 [38.75, 58.75]	50.50 [43.75, 60.75]	58.50 [38.25, 65.75]	0.769
N2 (%)		66.46 [57.32, 80.29]	60.69 [53.36, 64.69]	62.12 [56.89, 68.13]	64.05 [54.12, 68.33]	0.667
N3 (min)		3.75 [0.00, 19.88]	8.50 [4.06, 19,12]	11.50 [1.25, 20.62]	16.00 [3.50, 21.38]	0.608
N3 (%)		4.02 [0.00, 23.53]	12.36 [5.16, 23.46]	12.91 [1.81, 23.78]	15.02 [4.88, 23.66]	0.639
REM (min)		0.00 [0.00, 20.75]	12.25 [3.75, 17.56]	0 [0, 19.62]	15.00 [0.00, 16.12]	0.734
REM (%)		0.00 [0.00, 16.83]	12.16 [5.60, 14.58]	0 [0, 16.84]	14.88 [0.00, 17.28]	0.643

TES-TI can accurately target the thalamus

Figure 2B illustrates the spatial distribution of the simulated TI electric field within a participant's gray matter. The maximum field intensity was localized along the midline, encompassing both the left and right thalami. Within the target regions (i.e., bilateral thalami), the mean electric field magnitude was 1.25 ±

0.41 V/m, and the average focality was 1.12 ± 0.13. These values indicate that, during stimulation, the thalamus was exposed to an electric field of greater strength than the surrounding brain regions and of sufficient intensity to potentially elicit a physiological response.

To evaluate the consistency of stimulation efficacy across stimulation protocols, we compared the mean TI field intensity at the target and focality between the TES^{15kHz}-TI^{10Hz} and TES^{15kHz}-TI^{Peak} protocols. No significant differences were observed (intensity: $p = 0.125$; focality: $p = 0.340$), suggesting that any differences in the ability of these difference frequencies to evoke a response is unlikely to result from differences in targeting accuracy (Figures 2C–D).

TES^{15kHz}-TI^{10Hz} enhanced spindle activity during stimulation (STIM) compared to pre-stimulation activity (PRE)

To test the hypothesis that TES-TI targeted at the thalamus can enhance sleep spindle activity, we first examined sigma band power during STIM compared to PRE. As shown in Figure 3A, the TES^{15kHz}–TI^{10Hz} protocol was indeed associated with increase in sigma band power ($\Delta\tilde{x}_{STIM-PRE} = 0.49 \pm 0.82\ \log_{10}\ \mu V^2$, $p = 0.021$). This was not the case for any of the other stimulation protocols, including TES^{15kHz}-TI^{Peak} (Figure 3A). We additionally examined power within a narrow 10-Hz band (9.5–10.5 Hz) to assess whether the TES^{15kHz}–TI^{10Hz} stimulation could modulate neuronal activity at the same frequency; however, no significant difference was observed when comparing STIM and PRE ($\Delta\tilde{x}_{STIM-PRE} = 0.36 \pm 0.86\ \log_{10}\ \mu V^2$, $p = 0.15$).

We then examined the topography of the increase in sigma band power. Also as hypothesized, the cluster-based permutation analysis conducted in the TES^{15kHz}-TI^{10Hz} protocol revealed a significant positive cluster of 132 electrodes, showing increased sigma power in the frontal and centro-occipital regions (average p-value of electrodes surviving cluster correction = 0.022; Figure 3B).

Finally, we investigated changes in ISA. In the TES^{15kHz}-TI^{10Hz} protocol, ISA significantly increased during stimulation compared to the pre-stimulation period ($\Delta\tilde{x}_{STIM-PRE} = 7.48 \pm 12.90\ \mu V/s$, $p = 0.042$; Figure 3C).

No such effect was observed in the other stimulation protocols (TES^{15kHz}-TI^{Peak}: $\Delta\tilde{x}_{STIM-PRE}$ = –3.96 μV/s ± 17.31, p = 0.11; TES^{15kHz}: $\Delta\tilde{x}_{STIM-PRE}$ = –5.96 μV/s ± 8.97, p = 0.13).

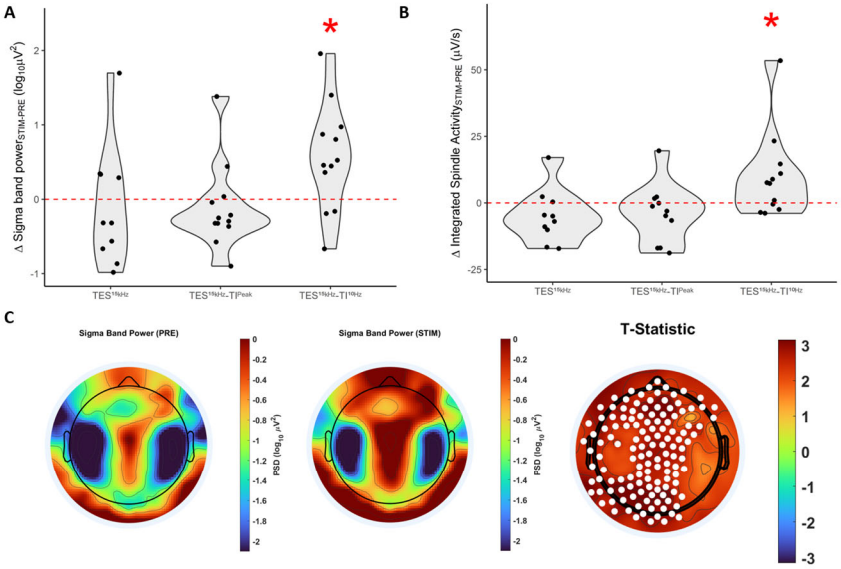

Figure 3. TES^{15kHz}-TI^{10Hz} stimulation enhances spindle activity. Distribution of the difference between the stimulation period (STIM) and the preceding three minutes (PRE) in sigma power (11-16Hz) (**A**) and integrated spindle activity (ISA) (**B**) across the stimulation protocols: TES^{15kHz}, i.e., kHz carrier frequency delivered without difference frequency; TES^{15kHz}-TI^{Peak} protocol, i.e., difference frequency matching individual participants' peak in the sigma range; TES^{15kHz}-TI^{10Hz} protocol, i.e., difference frequency of 10 Hz. Each data point in the plot corresponds to one participant. Red asterisks indicate significance (paired Wilcoxon test, p <0.05). **C,** topographical distribution of sigma power during PRE and STIM for the TES^{15kHz}-TI^{10Hz} stimulation protocol, along with the T-statistic topoplot of electrode comparisons (cluster-based permutation). Electrodes showing significant increases after cluster correction are marked in white.

Linear mixed effects models confirmed the significant increase in sigma band power and spindle features observed between STIM and PRE in the TES^{15kHz}–TI^{10Hz} protocol. We fit two mixed-effect models to directly compare the impact of the 10Hz difference stimulation with that of the active control conditions TES^{15kHz} and TES^{15kHz}-TI^{Peak}. STIM-PRE differences in sigma band power and ISA were used as dependent variables in the models. Stimulation protocol was included as a fixed effect, while participant ID was modeled as a random effect to account for repeated measures across protocols. The analysis revealed that the increase in both sigma band power from PRE to STIM was significantly greater for TES^{15kHz}–TI^{10Hz} compared to the TES^{15kHz} protocol (sigma band

power: β = 0.67 $\log_{10}\mu V^2$, p = 0.018; ISA:14.70 μV/s, p = 0.0077). Conversely, no significant difference emerged between the TES^{15kHz}-TI^{Peak} protocol and the TES^{15kHz} protocol (sigma band power: β = -0.014 $\log_{10}\mu V^2$, p = 0.28; ISA: -1.46 μV/s, p = 0.791). Results of the linear mixed effects models are presented in Table 3.

Table 2. Mixed-effects models were fitted using two outcomes: the increase in sigma power and the integrated spindle activity (ISA) during the stimulation period (STIM) compared to the preceding 3-minute interval (PRE). These models compared the TES^{15kHz}-TI^{10Hz} protocol with two active control conditions: the TES^{15kHz}-TI^{Peak} the TES^{15kHz} protocols. TES^{15kHz} row was left blank as it represents the reference for the comparison.

	Sigma band power ($\log_{10}$ μV²)			Integrated spindle activity (μV/s)		
	β	Std. Error	p	β	Std. Error	p
Intercept	-0.10	0.21	0.62	-4.96	4.07	0.224
TES^{15kHz}						
TES^{15kHz}-TI^{Peak}	-0.014	0.28	0.96	-1.46	5.52	0.791
TES^{15kHz}-TI^{10Hz}	0.67	0.28	0.018*	14.70	5.52	0.0077*

Significance code: * p < 0.05

Low-frequency EEG power increased and high-frequency power decreased in all protocols between PRE and STIM epochs, reflecting increasing sleep depth during N2

Our analyses are based on one or two stimulations per participant, administered exclusively during the N2 sleep stage. Owing to the deepening of sleep within the nap, N2 EEG spectral power is expected to change over time regardless of the stimulation protocol employed. This factor can be averaged out in overnight studies where multiple stimulations can be delivered at different points in a longer sleep episode[30]. To tease apart spectral changes attributable to the spontaneous evolution of N2 sleep from

those induced by TES-TI stimulation, we also compared two consecutive 3-minute intervals of N2 sleep extracted from the baseline nap, when no stimulation was delivered.

As expected, the second 3-minute interval exhibited a significant increase in delta band power ($\Delta\tilde{x}_{STIM-PRE}$ = 0.87 ± 1.14 $\log_{10}$ μV², p = 0.012), along with significant decreases in beta ($\Delta\tilde{x}_{STIM-PRE}$ = -0.70 ± 0.67 $\log_{10}$ μV², p = 0.00049) and gamma band power ($\Delta\tilde{x}_{STIM-PRE}$ = -0.38 ± 0.32 $\log_{10}$ μV², p = 0.0049). No significant change was observed in the sigma band ($\Delta\tilde{x}_{STIM-PRE}$ = -0.078 ± 0.89 $\log_{10}$ μV², p = 0.91). Comparable spectral changes were observed in the TES^{15kHz}-TI^{Peak} protocol (delta band: $\Delta\tilde{x}_{STIM-PRE}$ = 0.61 ± 0.85 $\log_{10}$ μV², p = 0.016; beta band: $\Delta\tilde{x}_{STIM-PRE}$ = -0.69 ± 0.45 $\log_{10}$ μV², p = 0.00098; gamma band: $\Delta\tilde{x}_{STIM-PRE}$ = -0.59 ± 0.59 $\log_{10}$ μV², p = 0.0049) and in the TES^{15kHz} protocol (delta band: $\Delta\tilde{x}_{STIM-PRE}$ = 1.33 ± 2.18 $\log_{10}$ μV², p = 0.0098; beta band: $\Delta\tilde{x}_{STIM-PRE}$ = -0.49 ± 0.72 $\log_{10}$ μV², p = 0.0098; gamma band: $\Delta\tilde{x}_{STIM-PRE}$ = -0.50 ± 0.66 $\log_{10}$ μV², p = 0.0020) without concomitant changes in the sigma band power (TES^{15kHz}-TI^{Peak}: $\Delta\tilde{x}_{STIM-PRE}$ = -0.27 ± 0.34 $\log_{10}$ μV², p = 0.30; TES^{15kHz}: $\Delta\tilde{x}_{STIM-PRE}$ = -0.32 ± 0.10 $\log_{10}$ μV², p = 0.39). Results are reported in Table 2 and displayed in Figure 4.

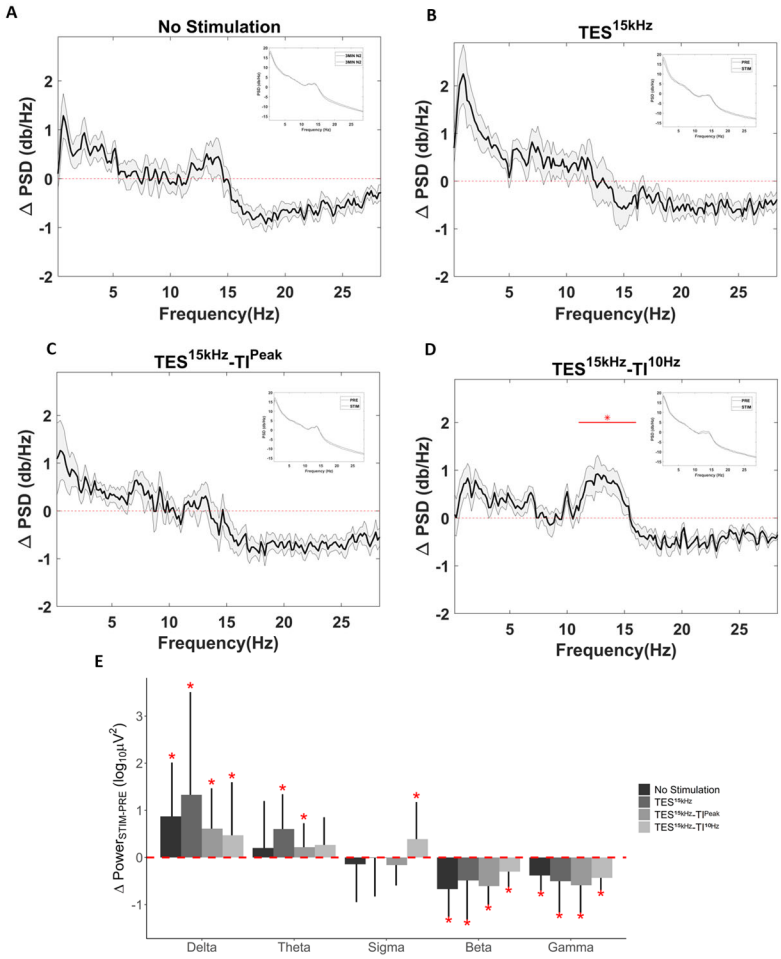

Figure 4. Changes in EEG spectral power changes across conditions. A, difference in power spectra between two consecutive 3-minute intervals of N2 during the baseline nap. **B,** difference in power spectra between STIM and PRE in the TES^{15kHz} protocol, i.e., kHz carrier frequency delivered without envelope frequency. **C,** difference in power spectra between STIM and PRE in the TES^{15kHz}-TI^{Peak} protocol, i.e., difference frequency matching individual participants' peak in the sigma range. **D,** difference in power spectra between STIM and PRE in the TES^{15kHz}-TI^{10Hz} protocol, i.e., difference frequency of 10 Hz. Average across electrodes, then across participants (dark line) and standard error of the mean difference (shaded light gray areas) are shown in each panel. The power spectra of the two intervals compared are displayed in the top right insert and they all exhibit a typical N2 sleep profile, with a dominant delta peak (slow waves) and a secondary sigma peak (spindles). **E,** changes in the frequency bands across the conditions at hand. Bar plots show the median difference, with error bars indicating interquartile range. Red asterisks indicate significance (paired Wilcoxon test, $p < 0.05$).

Table 3. Median and interquartile range of the EEG spectral power differences (log_{10} μV²) between a 3-minute stimulation interval and the preceding 3 minutes across three conditions: TES-TI with a 10 Hz difference frequency (TES^{15kHz}-TI^{10Hz}), TES-TI with a difference frequency matching the individual sigma peak (TES^{15kHz}-TI^{Peak}), kilohertz carrier frequency only (TES^{15kHz}); and a no-stimulation condition, using two consecutive N2 intervals from the baseline nap.

	TES^{15kHz}-TI^{10Hz}		TES^{15kHz}-TI^{Peak}		TES^{15kHz}		No Stimulation	
EEG band	$\Delta\tilde{x}$ ± IQR	p	$\Delta\tilde{x}$ ± IQR	p	$\Delta\tilde{x}$ ± IQR	p	$\Delta\tilde{x}$ ± IQR	p
Delta	0.47 ± 1.13	0.034*	0.61 ± 0.85	0.016*	1.33 ± 2.18	0.0098*	0.87 ± 1.14	0.012*
Theta	0.27 ± 0.60	0.052	0.22 ± 0.51	0.016*	0.60 ± 0.74	0.027*	0.20 ± 1.00	0.23
Sigma	0.49 ± 0.82	0.021*	-0.27 ± 0.34	0.30	-0.32 ± 0.10	0.49	-0.078 ± 0.89	0.91
Beta	-0.37 ± 0.31	0.00049*	-0.69 ± 0.45	0.00098*	-0.49 ± 0.72	0.0098*	-0.70 ± 0.67	0.00049*
Gamma	-0.43 ± 0.27	0.0015*	-0.59 ± 0.59	0.0049*	-0.50 ± 0.66	0.0020*	-0.38 ± 0.32	0.0049*

Significance code: * $p < 0.05$

Discussion

In this study, we demonstrated that TES-TI targeting the thalamus can effectively enhance spindle activity during a daytime sleep episode. We compared three minutes of stimulation (STIM) to the preceding three minutes (PRE) across three stimulation protocols: TES^{15kHz}-TI^{10Hz} (15 kHz carriers with a 10 Hz difference frequency); TES^{15kHz}-TI^{Peak} (15 kHz carriers with a difference frequency matched to each participant's peak within the sigma power band); TES^{15kHz} (15 kHz carriers with 0 Hz difference frequency). Data from an additional no stimulation control (two consecutive 3-minute N2 sleep intervals from baseline nap) were also analyzed to isolate changes in the EEG power spectrum attributable to increasing sleep depth during the nap. The results show that the TES^{15kHz}-TI^{10Hz} protocol significantly increased sigma power during STIM compared to PRE, while none of the other protocols did. Cluster-based permutation analysis localized this increase in 132 electrodes in the frontal and centro-posterior areas, a pattern consistent with typical spindle topography in healthy adults[36], supporting the role of TES-TI in enhancing spontaneous spindle generation. The increase in sigma power was associated with a significant increase in ISA, defined as the integrated absolute amplitude of the sleep spindles detected across all electrodes in a time interval of interest. Linear mixed effects models showed that the increase in both sigma band power and ISA during STIM compared to PRE was greater in the TES^{15kHz}-TI^{10Hz} compared the TES^{15kHz} protocol, while the TES^{15kHz}-TI^{Peak} stimulation failed to achieve the same effect.

Our experimental design employs a limited set of stimulations administered during N2 sleep within brief daytime nap episodes. This approach offers the simplicity necessary to assess the feasibility of a novel technique. However, this approach is susceptible to be confounded by shifts in the EEG power spectra associated with the progressive deepening of sleep within this stage in the course of a nap, a source of variability that would have been mitigated if multiple stimulation intervals at different points of a night sleep episode were averaged[30]. To disentangle possible time-related effects from those genuinely attributable to stimulation, we compared two consecutive 3-minute N2 intervals from the baseline nap, during which no stimulation was applied. In the second interval relative to the first, we observed an

increase in delta power and a decrease in beta and gamma power. Similar patterns, i.e., an increase in low-frequency power and a decrease in high-frequency power, were consistently observed across all experimental conditions. These spectral shifts are characteristic of the increasing sleep depth during N2 sleep[37], which often represents a transition state between "light" N1 sleep and "deep" N3 sleep[38]. This finding confirms that TES-TI stimulation preserves physiological sleep architecture while selectively acting on its target, namely spindle activity. This conclusion is also supported by the fact that nap-related metrics (i.e., sleep duration, sleep efficiency, wake after sleep onset, number of arousals, sleep stages) did not differ across conditions, indicating that TES-TI administration during sleep neither induced awakenings nor disrupted sleep architecture.

Unlike the TES^{15kHz}-TI^{10Hz} protocol, tailoring the difference frequency to the peak spindle frequency for each individual participant did not have any significant effect on spindle activity. Individualized stimulation frequencies offer potential advantages[39–41], even though these have not been borne out by studies that directly compared standardized and individualized frequencies using tACS, either during sleep[42] or during wakefulness[43]. In particular, it has been reported that tACS applied to the occipital cortex at a frequency slightly below the individual alpha peak maximized post-stimulation alpha power in the targeted region[43]. Moreover, recent electrophysiological investigations in rhesus monkeys using single-unit recordings indicate that TES-TI can effectively disrupt synchronized neuronal activity[44]. Thus, TES-TI applied at a difference frequency closely matching the optimal synchronization frequency of target neurons may be less effective or even counterproductive, whereas at nearby frequencies it may help entrain neuronal activity. The absence of a significant increase in the 9.5-10.5 Hz narrow band power, together with the increase in the sigma band (11Hz-16Hz) power during STIM compared with PRE in the TES^{15kHz}-TI^{10Hz} condition, supports this interpretation.

However, the mechanisms through which TES-TI acts inside the brain are still unclear. While initial models proposed selective neuronal sensitivity to the low frequency envelope via membrane lowpass filtering[23], subsequent work indicates that additional mechanisms, such as network level adaptation[45] or nonlinear

single cell frequency mixing mediated by voltage gated ion channels[46], are required, although these effects have been demonstrated only at field strengths exceeding those achievable in humans. Since the peak frequency for most subjects is considerably higher than 10Hz, it will be important to determine whether TES-TI in the fast spindle range, but outside the individual peak frequency, may also be effective.

The feasibility of using TES-TI to enhance sleep without compromising its integrity gives this technique advantages against other approaches explored to increase spindle activity. Z-drugs and benzodiazepine, among other side effects, have been associated with a reduction in slow wave sleep[18], while auditory stimulation can involuntarily cause awakening due to the high sensitivity of the thalamo-cortical complex to acoustic stimuli during sleep[21]. As shown by Lustenberger and colleagues[47], tACS applied to the frontal cortex within the sigma frequency range, in phase with spontaneously occurring spindles, can lead to increased post-stimulation sigma power and improve memory consolidation. TES-TI enabled us to overcome two limitations inherent to conventional TES approaches. First, tACS prevents simultaneous recording of EEG due to stimulation artifacts, whereas this is possible at the high carrier frequencies of TES-TI thanks to the use of hardware filters[30]. Second, conventional TES can induce scalp discomfort, possibly interfering with sleep maintenance, when trying to achieve an electrical field of intensity sufficient to induce a response in deep brain structures. This makes it unfeasible to elicit spindles by directly targeting the cerebral structures responsible for their generation, i.e., the thalamus[7,48]. The high frequency carrier employed in TES-TI allowed us to employ higher stimulation intensities without eliciting any sensation[25], and to enhance spindles by directly stimulating the site of their thalamic source deep inside the brain.

Strengths and limitations

This study provides evidence of effective non-invasive thalamic stimulation in humans. It also represents the first demonstration of TES-TI efficacy in enhancing spindle activity, validated across multiple active and inactive control conditions. Additionally, our findings confirm the feasibility of TES-TI administration during

sleep while concurrently recording EEG, paving the way for future studies testing its use in research and clinical settings. These results also support the specificity of TES-TI stimulation protocols with respect to both difference frequency and target region, as our previous study using TES-TI to target the ventromedial prefrontal cortex with a 1 Hz envelope frequency during sleep showed an increase in slow wave, but not spindle activity[30]. We utilized the open-source TI-Toolbox[31] platform to individualize electrode placement based on participants' T1- and T2-weighted MRI scans. Montage optimization was conducted to maximize the focality-intensity trade-off, ensuring that the thalamus received a stronger electric field than adjacent gray matter regions and that the field strength was sufficient to elicit a physiological response. Additionally, we ensured that intensity and focality were comparable across stimulation protocols, so that any observed differences in outcomes could not be attributed to variations in targeting quality of the ROI.

This initial study has obvious limitations. Stimulations were performed during an afternoon nap, which limited each experiment to one or two stimulations administered to each participant. The number of subjects is limited, reducing the power to detect weaker effects. Moreover, some subjects also received additional brief stimulations during REM sleep or during wakefulness, even if these are unlikely to have affected comparisons between STIM and PRE epochs within N2 and were counterbalanced among the various experiment conditions. While these findings serve as proof of concept for the capacity of thalamic TES-TI stimulation to elicit sleep spindles, their replication in studies employing multiple stimulation intervals across a full night of sleep is necessary. Moreover, further investigation is required to assess the potential impact of TES-TI induced spindle enhancement on memory consolidation and, more generally, on human cognition.

Conclusion

Bilateral thalamic stimulation via TES-TI during sleep stage N2 delivered with an envelope frequency of 10 Hz resulted in an enhancement of spindle activity localized to the expected scalp areas. The use of a

stimulation frequency matched with each participant's peak in the sigma band failed to achieve the same effect. Further research is required to understand the mechanisms of action of TES-TI in the thalamus, the possible cognitive effects of sleep spindles enhancement, and the potential applications of this technique in diseases associated with sleep spindle deficits (e.g., schizophrenia, Alzheimer's disease, Parkinson's disease, epilepsy).

Declaration of generative AI use

During the preparation of this work, the authors used Copilot for text and code editing. After using this tool, the authors reviewed and edited the content as needed and take full responsibility for the content of the published article.

Data and Code Availability

The data underlying this article will be shared on reasonable request to the corresponding authors. Customized codes used to create the main figures and tables have been made publicly available on GitHub, at https://github.com/sbruno3/TES-TI_spindles.

Acknowledgements

The TIBS-R investigational devices used in this project were provided by TI Solutions AG, Switzerland, as part of its Early Adopter Program (www.temporalinterference.com).

Funding

This project is funded by the Defense Advanced Research Projects Agency (DARPA) under cooperative agreement No. HR00112490326 (to G.T.). The content of the information does not necessarily reflect the position or the policy of the Government, and no official endorsement should be inferred.

Disclosure Statement

The authors declare no competing financial or non-financial interests, with the following exceptions: G.T. is Chair of Board and has a financial interest in Intrinsic Powers Inc., N.K. and E.N. are Board Members and have a financial interest in TI Solutions AG.

References

1. Loomis AL, Newton Harvey E, Hobart G. Potential Rhythms of the Cerebral Cortex during Sleep. *Science (1979)*. 1935;81(2111):597-598. doi:https://www.jstor.org/stable/1659223

2. Fernandez LMJ, Lüthi A. Sleep spindles: Mechanisms and functions. *Physiol Rev*. 2020;100(2):805-868. doi:10.1152/PHYSREV.00042.2018/ASSET/IMAGES/LARGE/Z9J0022029380013.JPEG

3. Andrillon T, Nir Y, Staba RJ, et al. Sleep Spindles in Humans: Insights from Intracranial EEG and Unit Recordings. *The Journal of Neuroscience*. 2011;31(49):17821. doi:10.1523/JNEUROSCI.2604-11.2011

4. Berry RB, Albertario CL, Harding SM, et al. *The AASM Manual for the Scoring of Sleep and Associated Events. Rules, Terminology and Technical Specifications. Version 2.5*. American Academy of Sleep Medicine; 2018.

5. Serantes D, Cavelli M, Gonzalez J, Mondino A, Benedetto L, Torterolo P. Characterising the power spectrum dynamics of the non-REM to REM sleep transition. *J Sleep Res*. 2025;34(3):e14388. doi:10.1111/jsr.14388

6. Bandarabadi M, Herrera CG, Gent TC, Bassetti C, Schindler K, Adamantidis AR. A role for spindles in the onset of rapid eye movement sleep. *Nature Communications 2020 11:1*. 2020;11(1):5247-. doi:10.1038/s41467-020-19076-2

7. Steriade M, Domich L, Oakson G, Deschenes M. The deafferented reticular thalamic nucleas generates spindle rhythmicity. *J Neurophysiol*. 1987;57(1):260-273. doi:10.1152/JN.1987.57.1.260,

8. Mölle M, Eschenko O, Gais S, Sara SJ, Born J. The influence of learning on sleep slow oscillations and associated spindles and ripples in humans and rats. *European Journal of Neuroscience*. 2009;29(5):1071-1081. doi:10.1111/J.1460-9568.2009.06654.X;CTYPE:STRING:JOURNAL

9. Lutz ND, Harkotte M, Born J. Sleep's contribution to memory formation. *Physiol Rev*. 2026;106(1):363-483. doi:10.1152/physrev.00054.2024

10. Ferrarelli F, Huber R, Peterson MJ, et al. Reduced sleep spindle activity in schizophrenia patients. *Am J Psychiatry*. 2007;164(3):483-492. doi:10.1176/AJP.2007.164.3.483

11. Weng YY, Lei X, Yu J. Sleep spindle abnormalities related to Alzheimer's disease: a systematic mini-review. *Sleep Med*. 2020;75:37-44. doi:10.1016/J.SLEEP.2020.07.044

12. Latreille V, Carrier J, Lafortune M, et al. Sleep spindles in Parkinson's disease may predict the development of dementia. *Neurobiol Aging*. 2015;36(2):1083-1090. doi:10.1016/J.NEUROBIOLAGING.2014.09.009

13. Bender AC, Jaleel A, Pellerin KR, et al. Altered Sleep Microarchitecture and Cognitive Impairment in Patients With Temporal Lobe Epilepsy. *Neurology*. 2023;101(23):E2376-E2387. doi:10.1212/WNL.0000000000207942

14. Ferrarelli F, Tononi G. Reduced sleep spindle activity point to a TRN-MD thalamus-PFC circuit dysfunction in schizophrenia. *Schizophr Res*. 2017;180:36-43. doi:10.1016/j.schres.2016.05.023

15. Leong CWY, Leow JWS, Grunstein RR, et al. A systematic scoping review of the effects of central nervous system active drugs on sleep spindles and sleep-dependent memory consolidation. *Sleep Med Rev*. 2022;62:101605. doi:10.1016/J.SMRV.2022.101605

16. Malkani RG, Zee PC. Brain Stimulation for Improving Sleep and Memory. *Sleep Med Clin*. 2020;15(1):101-115. doi:10.1016/J.JSMC.2019.11.002

17. Zhang J, Yetton B, Whitehurst LN, Naji M, Mednick SC. The effect of zolpidem on memory consolidation over a night of sleep. *Sleep*. 2020;43(11):zsaa084. doi:10.1093/SLEEP/ZSAA084

18. Dujardin S, Pijpers A, Pevernagie D. Prescription Drugs Used in Insomnia. *Sleep Med Clin*. 2018;13(2):169-182. doi:10.1016/J.JSMC.2018.03.001

19. Ngo HV V., Seibold M, Boche DC, Mölle M, Born J. Insights on auditory closed-loop stimulation targeting sleep spindles in slow oscillation up-states. *J Neurosci Methods*. 2019;316:117-124. doi:10.1016/J.JNEUMETH.2018.09.006

20. Antony JW, Paller KA. Using oscillating sounds to manipulate sleep spindles. *Sleep*. 2017;40(3). doi:10.1093/SLEEP/ZSW068,

21. Bellesi M, Riedner BA, Garcia-Molina GN, Cirelli C, Tononi G. Enhancement of sleep slow waves: underlying mechanisms and practical consequences. *Front Syst Neurosci*. 2014;8(October):208. doi:10.3389/FNSYS.2014.00208

22. Lustenberger C, Boyle MR, Alagapan S, Mellin JM, Vaughn B V., Fröhlich F. Feedback-Controlled Transcranial Alternating Current Stimulation Reveals a Functional Role of Sleep Spindles in Motor Memory Consolidation. *Current Biology*. 2016;26(16):2127-2136. doi:10.1016/J.CUB.2016.06.044

23. Grossman N, Bono D, Dedic N, et al. Noninvasive Deep Brain Stimulation via Temporally Interfering Electric Fields. *Cell*. 2017;169(6):1029-1041.e16. doi:10.1016/J.CELL.2017.05.024

24. Acerbo E, Jegou A, Luff C, et al. Focal non-invasive deep-brain stimulation with temporal interference for the suppression of epileptic biomarkers. *Front Neurosci*. 2022;16:945221. doi:10.3389/FNINS.2022.945221/BIBTEX

25. Thiele C, Tamm C, Ruhnau P, Zaehle T. Perceptibility and Pain Thresholds in Low- and High-Frequency Alternating Current Stimulation: Implications for tACS and tTIS. *Journal of Cognitive Enhancement 2024 9:1*. 2024;9(1):79-91. doi:10.1007/S41465-024-00304-2

26. Wang Y, Zeng GQ, Wang M, et al. The safety and efficacy of applying a high-current temporal interference electrical stimulation in humans. *Front Hum Neurosci*. 2024;18:1484593. doi:10.3389/FNHUM.2024.1484593/BIBTEX

27. Ray LB, Baena D, Fogel SM. "Counting sheep PSG": EEGLAB-compatible open-source matlab software for signal processing, visualization, event marking and staging of polysomnographic data. *J Neurosci Methods*. 2024;407. doi:10.1016/j.jneumeth.2024.110162

28. Delorme A, Makeig S. EEGLAB: An open source toolbox for analysis of single-trial EEG dynamics including independent component analysis. *J Neurosci Methods*. 2004;134(1):9-21. doi:10.1016/j.jneumeth.2003.10.009

29. Botzanowski B, Acerbo E, Lehmann S, et al. Focal control of non-invasive deep brain stimulation using multipolar temporal interference. *Bioelectron Med*. 2025;11(1). doi:10.1186/S42234-025-00169-6

30. Schaeffer EL, Haber I, Fan Z, et al. Enhancement of Sleep Slow Wave Activity using Transcranial Electrical Stimulation with Temporal Interference. *medxriv*. Published online 2025. doi:10.1101/2025.08.11.25333452

31. Haber I, Jackson A, Thielscher A, Hai A, Tononi G. TI-Toolbox: An open-source software for temporal interference stimulation research. *Brain Stimul*. 2026;19(1):103016. doi:10.1016/J.BRS.2025.103016

32. Vallat R, Walker MP. An open-source, high-performance tool for automated sleep staging. *Elife*. 2021;10. doi:10.7554/ELIFE.70092,

33. Lacourse K, Delfrate J, Beaudry J, Peppard P, Warby SC. A sleep spindle detection algorithm that emulates human expert spindle scoring. *J Neurosci Methods*. 2019;316:3-11. doi:10.1016/j.jneumeth.2018.08.014

34. Maris E, Oostenveld R. Nonparametric statistical testing of EEG- and MEG-data. *J Neurosci Methods*. 2007;164(1):177-190. doi:10.1016/j.jneumeth.2007.03.024

35. Fattinger S, De Beukelaar TT, Ruddy KL, et al. Deep sleep maintains learning efficiency of the human brain. *Nat Commun*. 2017;8:15405. doi:10.1038/NCOMMS15405

36. Zeitlhofer J, Gruber G, Anderer P, Asenbaum S, Schimicek P, Saletu B. Topographic distribution of sleep spindles in young healthy subjects. *J Sleep Res*. 1997;6(3):149-155. doi:10.1046/J.1365-2869.1997.00046.X;PAGE:STRING:ARTICLE/CHAPTER

37. Hussain I, Hossain MA, Jany R, et al. Quantitative Evaluation of EEG-Biomarkers for Prediction of Sleep Stages. *Sensors 2022, Vol 22, Page 3079*. 2022;22(8):3079. doi:10.3390/S22083079

38. Anderer P, Gruber G, Parapatics S, et al. An E-Health Solution for Automatic Sleep Classification according to Rechtschaffen and Kales: Validation Study of the Somnolyzer 24 × 7 Utilizing the Siesta Database. *Neuropsychobiology*. 2005;51(3):115-133. doi:10.1159/000085205

39. Vosskuhl J, Strüber D, Herrmann CS. Non-invasive Brain Stimulation: A Paradigm Shift in Understanding Brain Oscillations. *Front Hum Neurosci*. 2018;12. doi:10.3389/FNHUM.2018.00211,

40. Stecher HI, Herrmann CS. Absence of alpha-tACS aftereffects in darkness reveals importance of taking derivations of stimulation frequency and individual alpha variability into account. *Front Psychol*. 2018;9(JUN). doi:10.3389/FPSYG.2018.00984,

41. Frohlich F, Riddle J. Conducting double-blind placebo-controlled clinical trials of transcranial alternating current stimulation (tACS). *Transl Psychiatry*. 2021;11(1). doi:10.1038/S41398-021-01391-X

42. Ladenbauer J, Khakimova L, Malinowski R, et al. Towards Optimization of Oscillatory Stimulation During Sleep. *Neuromodulation: Technology at the Neural Interface*. 2023;26(8):1592-1601. doi:10.1016/J.NEUROM.2022.05.006

43. Vossen A, Gross J, Thut G. Alpha Power Increase After Transcranial Alternating Current Stimulation at Alpha Frequency (α-tACS) Reflects Plastic Changes Rather Than Entrainment. *Brain Stimul*. 2015;8(3):499-508. doi:10.1016/J.BRS.2014.12.004

44. Vieira PG, Krause MR, Pack CC. Temporal interference stimulation disrupts spike timing in the primate brain. *Nat Commun*. 2024;15(1):1-13. doi:10.1038/S41467-024-48962-2;TECHMETA=120,9;SUBJMETA=1453,1647,378,631;KWRD=ELECTROPHYSIOLOGY,NEUROSCIENCE

45. Esmaeilpour Z, Kronberg G, Reato D, Parra LC, Bikson M. Temporal interference stimulation targets deep brain regions by modulating neural oscillations. *Brain Stimul*. 2021;14(1):55-65. doi:10.1016/j.brs.2020.11.007

46. Plovie T, Schoeters R, Tarnaud T, Joseph W, Tanghe E. Nonlinearities and timescales in neural models of temporal interference stimulation. *Bioelectromagnetics*. 2025;46(1). doi:10.1002/BEM.22522

47. Lustenberger C, Boyle MR, Alagapan S, Mellin JM, Vaughn B V., Fröhlich F. Feedback-controlled transcranial alternating current stimulation reveals functional role of sleep spindles in motor memory consolidation. *Curr Biol*. 2016;26(16):2127. doi:10.1016/J.CUB.2016.06.044

48. Steriade M, Deschenes M, Domich L, Mulle C. Abolition of spindle oscillations in thalamic neurons disconnected from nucleus reticularis thalami. *J Neurophysiol*. 1985;54(6):1473-1497. doi:10.1152/JN.1985.54.6.1473,